Published in final edited form as:

Cancer Res. 2023 May 02; 83(9): 1503–1516. doi:10.1158/0008-5472.CAN-22-1821.

Spatial transcriptomics depict ligand-receptor crosstalk heterogeneity at the tumor-stroma interface in long-term ovarian cancer survivors

Sammy Ferri-Borgogno[1,†], **Ying Zhu**[2,3,†], **Jianting Sheng**[2,3], **Jared K. Burks**[4], **Javier A. Gomez**[4], **Kwong Kwok Wong**[1], **Stephen T.C. Wong**[2,3,*], **Samuel C. Mok**[1,*]

[1]Department of Gynecologic Oncology and Reproductive Medicine, The University of Texas MD Anderson Cancer Center, Houston, TX 77030, USA

[2]Systems Medicine and Bioengineering Department, Houston Methodist Cancer Center, Houston Methodist Hospital, Houston, TX 77030, USA

[3]Departments of Pathology and Laboratory Medicine and Radiology, Houston Methodist Hospital, Weill Cornell Medicine, Houston, TX 77030, USA

[4]Department of Leukemia, The University of Texas MD Anderson Cancer Center, Houston, TX 77030, USA

Abstract

Advanced high-grade serous ovarian cancer (HGSC) is an aggressive disease that accounts for 70% of all ovarian cancer deaths. Nevertheless, 15% of patients diagnosed with advanced HGSC survive more than 10 years. The elucidation of predictive markers of these long-term survivors (LTS) could help identify therapeutic targets for the disease, and thus improve patient survival rates. To investigate the stromal heterogeneity of the tumor microenvironment (TME) in ovarian cancer, we used spatial transcriptomics to generate spatially resolved transcript profiles in treatment naïve advanced HGSC from LTS and short-term survivors (STS) and determined the association between cancer-associated fibroblasts (CAF) heterogeneity and survival in patients with advanced HGSC. Spatial transcriptomics and single-cell RNA sequencing data were integrated to distinguish tumor and stroma regions, and a computational method was developed to investigate spatially resolved ligand-receptor interactions between various tumor and CAF subtypes in the TME. A specific subtype of CAFs and its spatial location relative to a

[*]Co-corresponding authors: Samuel C. Mok, PhD, Department of Gynecologic Oncology and Reproductive Medicine, Unit 1362, The University of Texas MD Anderson Cancer Center, 1515 Holcombe Blvd, Houston, TX 77030, USA; Phone: 713-792-1442; scmok@mdanderson.org; Stephen T.C. Wong, PhD, Systems Medicine and Bioengineering Department, Houston Methodist Cancer Center, Houston Methodist Hospital, 6670 Bertner Ave, Room 6-211, Houston, TX 77030, USA; Phone: 713-441-5884; stwong@houstonmethodist.org.

[†]These authors contributed equally.

AUTHOR CONTRIBUTIONS

S.F.-B., Y.Z., S.T.C.W. and S.C.M., designed the study and planned the experiments. S.F.-B. conducted most of the experiments and analyzed the mIF data; Y.Z. analyzed the ST and scRNA-seq data. J.S., J.K.B., J.G., K.K.W. and S.T.C.W., provided intellectual contributions to experimental design and data analysis. S.F.-B. and Y.Z., wrote the initial draft of the manuscript. S.F-B., Y.Z., S.T.C.W., and S.C.M., prepared and revised the manuscript. All authors have read and agreed to the published version of the manuscript. The authors declare that they have no competing interests.

CONFLICT OF INTEREST

The authors declare no potential conflicts of interest.

particular ovarian cancer cell subtype in the TME correlated with long-term survival in advanced HGSC patients. Also, increased APOE-LRP5 crosstalk occurred at the stroma-tumor interface in tumor tissues from STS compared to LTS. These findings were validated using multiplex immunohistochemistry. Overall, this spatial transcriptomics analysis revealed spatially resolved CAF-tumor crosstalk signaling networks in the ovarian TME that are associated with long-term survival of HGSC patients. Further studies to confirm whether such crosstalk plays a role in modulating the malignant phenotype of HGSC and could serve as a predictive biomarker of patient survival are warranted.

Keywords

Ovarian cancer; long-term survivors; spatial transcriptomics; CAF heterogeneity; ligand-receptor cross-talk

INTRODUCTION

High-grade serous ovarian cancer is the major subtype of epithelial ovarian cancer and appears to arise from the ovarian surface epithelium or the fallopian tube epithelium (1). It accounts for more than 70% of ovarian cancer deaths making it the most lethal gynecologic malignancy (2). HGSC typically presents as aggressive advanced-stage disease (3) and is initially sensitive to platinum-and-taxane–based chemotherapy. However, the vast majority of patients with advanced HGSC (>75-80%) have recurrence after initial treatment, experience rapid disease progression, and die of progressively chemotherapy-resistant disease (4,5). Nevertheless, 15% of patients diagnosed with advanced HGSC have overall survival (OS) durations of more than 10 years (6,7).

Reports to date have not fully established the heterogeneity of the tumor microenvironment (TME) in ovarian cancer and its association with clinical outcomes. The TME, which is composed primarily of fibroblasts, endothelial cells, lymphocytic infiltrates, and extracellular matrix proteins, can directly affect cancer cell growth, migration, and differentiation and thus presents a unique opportunity for cancer diagnosis and treatment (8). The immune system is an important determinant of the TME; ongoing inflammation results in various immunologic gene products that create a favorable microenvironment for tumor growth and progression (9–13), and the presence of specific immune cell types, such as intratumor $CD8^+$ T cells, is associated with improved survival in patients with various types of cancer, including ovarian cancer (9,10,14,15). These findings suggest that immune cell heterogeneity plays an important role in conferring the malignant phenotypes of cancer cells. In addition to immune cell heterogeneity, cancer-associated fibroblast (CAF) heterogeneity may also play essential roles in modulating tumor growth. CAFs are characterized by their expression of traditional markers, including alpha-smooth muscle actin (αSMA), S100A4, vimentin (VIM), fibroblast activation protein (FAP), and platelet-derived growth factor receptor alpha (PDGFRα) and beta (PDGFRβ) (16). Differential expression of these CAF markers has recently been found in the TME of pancreatic cancer (17). Furthermore, TME has been found to contain additional CAF subtypes that have distinct biomarker expression profiles and cellular functions that differ from those of CAFs outside the TME (18,19).

However, the molecular mechanisms underlying the promotion or inhibition of cancer by various CAF subtypes as well as the interplay between different CAF populations and their spatial locations within the TME in ovarian cancer are not fully understood.

Recent innovations in high-throughput analyses of patient-derived specimens may address the clinical challenges described above. The use of integrated “multi-omics” platforms has improved our understanding of how genetic changes affect the gene expression profiles (20–22). However, because most of the data generated with these platforms are derived from bulk tumor tissue, they have limited utility in the clinical management of HGSC. Previous studies have shown that the stroma admixture affects the interpretation and reproduction of molecular subtypes and gene signatures derived from bulk tissue (23). Recently, researchers used single-cell RNA-seq (scRNA-seq) analyses to characterize the heterogeneity of the HGSC TME, thereby providing valuable information about different HGSC subtypes and potential novel therapeutic approaches (24–26). scRNA-seq has also been integrated with whole-genome sequencing to reveal that mutational signatures drive site-specific immune evasion in HGSC (27). However, the aforementioned techniques and analyses cannot provide spatial information. Increasing evidence in multiple cancer types suggests that the spatial location of various cellular components of the TME and their position in relation to tumor cells, immune cells, and blood vessels can modulate anti- and pro-tumor responses (28–31). Single cell spatial proteomic data analysis has provided insights into the spatial heterogeneity of the TME of HGSC (13,32), but limited by the number of simultaneously labelled markers.

Spatial transcriptomics technology, which captures genome-wide readouts across biological tissue space, enables researchers to determine how genes are spatially expressed in the complex TME (33). In this study, we used spatial transcriptomics to identify spatially-resolved CAF associated biomarkers which may have prognostic significance in HGSC. We integrated spatial transcriptomics with scRNA-seq to distinguish tumor and stroma regions. In addition, we developed a method to investigate region-specific ligand-receptor interactions between HGSC and neighboring CAF subregions and subsequently identified a ligand-receptor pair in a subtype of CAFs and their neighboring HGSC cells that has prognostic significance.

MATERIALS AND METHODS

Patient samples

A total of 4 frozen and 42 paraffin-embedded tumor tissue samples obtained from patients with advanced (stage IIIB-IV) HGSC were used in the spatial transcriptomics and multiplexed immunofluorescence (mIF) experiments, respectively. The clinicopathological characteristics of samples used in the study were summarized in supplementary table 1. They were collected from previously untreated patients undergoing primary cytoreductive surgery for ovarian cancer. All samples and clinical data were obtained from the ovarian cancer repository of the Department of Gynecologic Oncology and Reproductive Medicine under protocols approved by the University of Texas MD Anderson’s Institutional Review Board. Written informed consent from the patients were obtained by front desk personnel, and the studies were conducted in accordance with recognized ethical guidelines.

Spatial transcriptomics

Spatial transcriptomics experiments were performed according to the manufacturer's protocol (10x Genomics). Briefly, a 10-μm-thick HGSC tissue frozen section was placed onto a spatial transcriptomics expression slide to fit an 8 x 8 mm spatially barcoded array with 1007 spots, each with a diameter of 100 μm and a center-to-center distance of 200 μm. The pooled barcoded and spatially transcribed cDNA libraries for each sample were sequenced using Illumina NextSeq500 flow cells at MD Anderson's Advanced Technology Genomics Core. Raw output base call (BCL) files from the sequencer were demultiplexed into fastq files (10x Genomics).

CAF annotation

The CAF clusters were annotated if the stroma clusters significantly expressed the traditional CAF markers ($p < 0.01$). For investigating the CAF heterogeneity across samples, the average log fold-change of the CAF genes in each CAF cluster was computed as the log fold-change of the average gene expression in that CAF cluster compared to the average gene expression in all other clusters in that sample.

Multimodal intersection analysis

With the gene sets extracted from spatial transcriptomics and scRNA-seq modalities, the overlap between the region-specific (differentially expressed genes as identified in spatial transcriptomics data analysis above) and cell type specific gene sets (differentially expressed genes as identified in scRNA-seq analysis above) was computed. A hypergeometric test was performed to identify the significant enrichment (using a threshold of $p < 1 \times 10^{-10}$) of any specific cell type within a tumor/stroma subregion (34) using 16,522 background genes. For the immune cells, the hypergeometric test was performed by computing the overlap between the top 150 differentially expressed genes (avg_logFC>0.25, p<10-5) of the immune cell subtypes and the differentially expressed genes (avg_logFC >0, p<0.01) of tumor, CAF and other stroma clusters of ST data. The $-\log_{10}$(p-value) of the hypergeometric test was computed as the enrichment score and compared between the LTS and STS for tumor or CAF clusters.

Ligand receptor interaction analysis

Using the CCCExplorer modeling tool as described in Choi et al. and Yeung et al. (35,36), which included 2,671 ligand-receptor pairs and a comprehensive signaling pathway database, ligand-receptor interactions were determined at the interface between every stroma and tumor subregion. At each interface, only the stroma spots and tumor spots nearest to the interface were considered. The minimum distance of each stroma spot to the tumor, and the minimum distance of each tumor spot to the stroma were equal to the minimum distance between the ST spots, that is, 200 μm. Details of the ligand receptor interaction analysis are provided in the Supplementary Data.

Statistical analysis

A non-parametric Wilcoxon rank sum test was used to detect differences in the mean intensities/stroma area ratios and positive cells/total cells ratios between LTS and STS

samples in the mIF experiments, and to identify the differentially expressed genes in the spatial transcriptomics and scRNA-seq data analyses. A p-value less than 0.05 was considered statistically significant. For the analyses of differentially expressed genes of ST and scRNA-seq, adjusted p-value was computed based on bonferroni correction using all genes in the dataset.

Data availability

All data needed to evaluate the conclusions in the paper are present in the paper and/or the Supplementary Materials. The scRNA-seq datasets were downloaded from GEO database under accession GSE118828 (37) and GSE158722 (38). Other raw data are available upon reasonable request from the corresponding author.

Additional Methods are available in Supplementary Data

RESULTS

Generation of spatially resolved RNA-seq profiles of HGSC tumors

Spatial transcriptomics analysis was performed on four samples of treatment-naïve advanced HGSC (Fig. 1A). Each spatial transcriptomics spot captured approximately 20-50 cells. After alignment of fastq file using Cell Ranger (10x Genomics), an average of 3,400 distinct genes were detected in each spot. Each sample was then loaded into R Seurat package and normalized by SCTransform. Clustering was then performed by FindClusters (R Seurat) based on the shared nearest-neighbor modularity optimization algorithm (39) using the first 10 dimensions of principal component analysis. Differentially expressed genes with significantly higher expression in each spatial transcriptomics cluster than others were identified ($p < 0.01$, Wilcoxon rank sum test and average log fold-change > 0) (Supplementary Fig. 1A, B and Supplementary Table 2). Publicly available scRNA-seq data from Shih et al. (37) were analyzed and used to define differentially expressed genes for the major cell types. (Fig. 1B, Supplementary Table 3).

With the differentially expressed genes extracted across the scRNA-seq and spatial transcriptomics modalities, the overlap between each pair of cell type-specific and region-specific gene sets was computed by multimodal intersection analysis (MIA) (34). A hypergeometric test was performed to assess significant enrichment using a threshold of $p < 10^{-10}$ (Fig. 1C); for example, tumor clusters were assigned if the enrichment p-value of any of the epithelial cell types Ep_1 ($SPON1^+$), Ep_2 (SST^+), Ep_3 ($ATHL1^+$), or Ep_4 ($TPPP3^+$) (Supplementary Table 2) in that cluster was lower than 10^{-10}. Stroma clusters were assigned if they were not tumor clusters. From the MIA map, we observed the infiltration of immune cells in some tumor clusters (e.g., B cells were enriched in clusters LTS#1_c5 and LTS#1_c2). The similarity among clusters across the four samples was measured by Pearson correlation of the differentially expressed genes and is presented in the correlation heatmap (Supplementary Fig. 1C).

A second publicly available scRNA-seq dataset from Azizi et al. (40) was analyzed and used to define differentially expressed genes for the immune cell types and MIA analysis was then performed as described above (Supplementary Fig. 2). Top differentially enriched cell

types in the tumor compartment were $CD8^+$EM, B_cells1, NK1, $CD4^+$CM among the T/B cells subgroup and Monocyte1, mDC and pDC1 among myeloid cell types. CAF clusters did not reveal any difference in the presence of immune cells between STS and LTS. These findings suggest that LTS samples have an enrichment of tumor infiltrating immune cells compared to STS samples.

Overrepresentation analysis of selected gene ontology (GO) biological process terms showed the difference between tumor and stroma clusters (Fig. 1D and Supplementary Fig. 3). Tumor clusters were highly enriched with metabolic processes (e.g., cellular/RNA metabolism), cellular respiration, and cell cycle processes. Stroma clusters were highly enriched with biological processes of cell motility/migration, extracellular matrix organization/disassembly, vasculature development, and immune responses (Fig. 1D and Supplementary Fig. 3).

Identification and mapping of tumor and stroma cell clusters

To verify the accuracy of our tumor/stroma classification by enrichment analysis of spatial transcriptomics RNA-seq data, the normalized expression of major tumor and stroma markers was mapped for each sample and overlaid them on the H&E images. We confirmed that the normalized expression of the tumor markers WFDC2, MUC16, and CLDN4 was localized to the tumor regions and that the normalized expression of COL1A1, VIM, and FN1 was restrained to the stroma regions (Fig. 2A and Supplementary Fig. 4).

After the clustering of spatial transcriptomics spots, we discovered a high level of heterogeneity among the four tumor samples and annotated the tumor and stroma clusters (Fig. 2B). Tumor clusters STS#1_c2 and STS#2_c1 (identified in patients STS#1 and STS#2) were characterized by the increased expression of CDK1 (Supplementary Table 2), one of the most important regulators of cell cycle progression in mammalian cells. Moreover, tumor clusters STS#1_c2 and STS#2_c0 expressed high levels of LGR5 (Supplementary Table 2), which promotes cancer cell mobility, tumor formation, and epithelial-mesenchymal transition through the activation of Wnt/β-catenin signaling. In contrast, neither CDK1 nor LGR5 were detected in any of tumor clusters in patients LTS#1 and LTS#2. Moreover, most of the tumor clusters in all four samples expressed WFDC2, a gene commonly overexpressed in ovarian carcinomas compared with normal ovarian tissues (41).

Heterogeneity of stroma subclusters

Analysis of the stroma clusters from patients STS#1 and STS#2 showed that the stroma clusters STS#1_c0 and STS#2_c4, which were located near the tumor edge, expressed high levels of COL1A1 and periostin (POSTN), whereas stroma clusters STS#1_c1 and STS#2_c3, which were located distant from the tumor edge, expressed high levels of COL1A1 and CD36 (Fig. 2B, left panel). Stroma clusters STS#1_c4 and STS#2_c2, which were closely surrounded by tumor clusters, expressed high levels of periostin. In contrast, high levels of periostin were identified in only a single stroma cluster, LTS#1_c7, surrounding the tumor cluster LTS#1_c5 in patient LTS#1 and in a single stroma cluster, LTS#2_c0, surrounding the tumor cluster LTS#2_c5 in patient LTS#2. In addition, only

stroma cluster LTS#2_c4 in patient LTS#2 expressed CD36 (Fig. 2B, right panel). These data suggest both intra- and inter-stromal heterogeneity among HGSCs. Moreover, tumors derived from patients STS#1 and STS#2 were distinct from those derived from patients LTS#1 and LTS#2. Indeed, survival analysis demonstrated that patients LTS#1 and LTS#2 were long-term survivors (LTSs) with overall survival durations of more than 120 months, whereas patients STS#1 and STS#2 were short-term survivors (STSs) with overall survival durations of less than 24 months. Furthermore, tumor samples from LTSs had lower levels of stromal periostin and CD36 expression.

To further elucidate stromal heterogeneity and the relationship between traditional CAF markers and the stroma clusters, we assessed the expression of traditional CAF markers, including αSMA (ACTA2), S100A4, VIM, FAP, PDGFRα (PDGFRA), and PDGFRβ (PDGFRB), in the stroma clusters we identified. Because we demonstrated that stromal CD36 and periostin were associated with STS (samples STS#1, STS#2) (Fig. 2B), which indicated a more aggressive phenotype of the stroma clusters, we included these markers in our CAF gene panel. Only 2 of the 6 stroma clusters in both the LTS samples (LTS#1 and LTS#2) expressed the traditional CAF markers, whereas all the stroma clusters in the STS samples (STS#1 and STS#2) expressed the CAF markers (Fig. 3A). These findings suggest these stroma clusters are enriched with CAFs in the tumor tissue and only a small percentage of stroma clusters in LTS tumors are enriched with CAFs. The stroma clusters that did not express CAF markers may be enriched with quiescent fibroblasts, mesenchymal cells, or other stromal cell types. In the two STS samples, the CAF clusters expressed a different set of CAF markers, and most expressed a majority of the eight CAF markers. In contrast, in the two LTS samples, all the stroma clusters that had CAF marker expression expressed a minority of the eight CAF markers. (Fig. 3A–C and Supplementary Fig. 5). These findings suggest intra- and inter-tumor CAF heterogeneity in HGSC and that tumors with enriched CAF clusters expressing multiple CAF markers may be associated with short-term survival.

Next, we examined the spatial distribution of various CAF clusters and the key molecules used for their annotation relative to the tumor clusters by plotting the average expression of each CAF marker as a function of the distance to tumor (Supplementary Fig. 5C). CAF clusters in the neighborhood of the tumor clusters (e.g., STS#1_c0, STS#1_c4, and LTS#1_c7) expressed high levels of periostin (Fig. 3B, C and Supplementary Fig. 5). Furthermore, CAF clusters located distant from the tumor clusters (e.g., STS#1_c1 and LTS#2_c4) expressed high levels of CD36. These findings suggest that spatially resolved CAF subpopulations in the ovarian TME may play different roles in conferring the malignant phenotypes of the tumor cells.

Prognostic significance of CD36 and periostin

Because the spatial transcriptomics data demonstrated that the overall periostin and CD36 expression levels in the CAF clusters of the 2 STS samples were markedly higher than those in the 2 LTS samples, we performed multiplexed immunofluorescence (mIF) analysis to quantify the spatial expression of periostin and CD36 in an independent set of 42 advanced HGSC cases (16 LTS and 26 STS) to verify our findings. Measuring the mean intensity of the selected markers in only the stroma areas demonstrated that STS samples had

significantly higher periostin expression levels near the stroma-tumor interface than LTS samples did ($p = 0.0069$) (Fig. 4A, B), suggesting spatially resolved periostin expression may serve as a prognostic marker. In addition, CD36 expression levels in the stroma areas distant from the tumor clusters were markedly higher in STS samples than they were in LTS samples, but this difference was not statistically significant ($p = 0.0675$) (Fig. 4C, D).

To validate the presence of a unique set of CAFs in STS samples compared to LTS samples and to validate our spatial transcriptomics findings showing that STS samples have markedly increased CAF clusters expressing all three markers (VIM, αSMA, and PDGFRB), we performed mIF analysis of these markers. We calculated the density of typical CAFs, expressing VIM, αSMA, and PDGFRB, by normalizing their number with the total number of stromal cells. We found a significantly higher density of $\alpha SMA^{+}VIM^{+}PDGFR\beta^{+}$ cells in the stroma of STS samples than in the stroma of LTS samples ($p < 0.001$) (Fig. 4E, F). The density of $\alpha SMA^{+}VIM^{+}$ ($PDGFR\beta^{-}$) cells, which represent myofibroblasts, did not differ between the STS and LTS samples ($p = 0.25$) (Fig. 4E, G). These results suggest that the spatially resolved CAF subpopulations expressing POSTN and αSMA, VIM, and PDGFRB in the ovarian TME may play a major role in conferring a more aggressive type of HGSC with decreased overall survival.

Crosstalk signaling network analysis

To characterize region-specific ligand-receptor interactions between CAFs and tumor cells, crosstalk signaling network analysis was performed (see Methods and Supplementary Methods). For each tumor and CAF cluster in each sample, we selected only the nearest neighboring spots on the interface and performed ligand-receptor analysis (Fig. 5A). In total, 84 and 50 distinct ligand-receptor pairs at the stroma-tumor interfaces of STS and LTS samples were identified, respectively (Supplementary Fig. 6–8). For example, we found APOE (ligand; on CAF) and LRP5 (receptor; on tumor) at the STS#1_c0-STS#1_c2 interface and the STS#2_c4-STS#2_c5 interface; and found THBS2 (ligand; on CAF) and CD47 (receptor; on tumor) at the STS#1_c0-STS#1_c6 interface (Fig. 5B,C and Supplementary Fig. 9). The region-specific ligand-receptor interaction networks between adjacent stroma and tumor subregions are shown in Fig. 5D. Sixty distinct ligand-receptor pairs were identified and pooled from the stroma-tumor interfaces between every stroma and tumor cluster in sample STS#1 (Fig. 5E). For example, each of the stroma ligands (APOE, THBS2, FN1) may bind to a more than one receptor of tumor. On the other hand, tumor receptors, such as ITGB1, and ITGB8 likely receive signals from multiple stromal ligands in sample STS #1 (Fig. 5E). The ligand-receptor interaction pattern on the stroma-tumor interfaces clearly showed between-sample differences (Fig. 5E, Supplementary Fig. 6–8). Searching for ligand-receptor pairs that have been shown to be associated with cancer patient prognosis, and metastatic process, we identified 9 ligand-receptor pairs associated with STS samples (APOE-LRP5, THBS2-CD47, PLAU-PLAUR, WNT10A-FZD5/FZD7, TGFB1-ENG/ACVRL1, IGF1-IGF1R, SEMA3C-NRP2) and 1 ligand-receptor pair associated with LTS samples (A2M-LRP1) (Fig. 5B, C and Supplementary Fig. 9).

Because the ligand-receptor pair APOE-LRP5 was found in the subcluster interface of both STS samples, we used mIF analysis to validate the presence of this interaction in

tumor samples obtained from the same cohort of LTS patients (n = 16) and STS patients (n = 26) used for CD36 and periostin staining as described above. Tissue samples were stained for COL1A1, LRP5, and APOE. The number of $LRP5^+$ cells and the mean intensity of APOE expression was calculated at the stroma-tumor interface. Spearman correlation analysis revealed a significant positive correlation between $LRP5^+$ cell density and APOE expression intensity at the stroma-tumor interface of STS samples ($r = 0.5904$, $p = 0.0015$) (Fig. 6A, B) but not LTS samples ($r = -0.2843$, $p = 0.2678$) (Fig. 6A, C). Moreover, no correlation between $LRP5^+$ cells in tumor areas and APOE expression intensity in stroma areas (excluding the stroma-tumor interface area) in either STS or LTS samples was found ($r = -0.07487$, $p = 0.7162$ and $r = -0.2279$, $p = 0.3774$, respectively) (Supplementary Fig. 10A). Furthermore, there was no significant correlation between APOE expression intensity and $LRP5^+$ cells in either the tumor or stroma areas of STS samples ($r = -0.1241$, $p = 0.5458$ and $r = -0.3464$ and $p = 0.0830$, respectively) or LTS samples ($r = -0.3088$, $p = 0.2273$ and $r = -0.1029$ and $p = 0.6943$, respectively) (Supplementary Fig. 10B, C). These data suggest that significant APOE-LRP5 crosstalk occurs at the stroma-tumor interface only, and that such crosstalk plays a crucial role in modulating the malignant phenotype of HGSC, which could serve as a predictive biomarker of patient survival.

To determine the functional role of APOE-LRP5 crosstalk in modulating the malignant phenotype of HGSC, HGSC cells expressing high levels of endogenous LRP5 were treated with physiological levels of purified APOE. A panel of HGSC cell lines was first screened for LRP5 expression by qRT-PCR (Supplementary Fig. 11A). OV90 cell line expressing highest levels of endogenous LRP5 was selected for further studies. The results showed that APOE-treated OV90 cells has a significantly higher growth rate than the control, and the stimulating effect of APOE was abrogated in OV90 cells transfected with LRP5-specific siRNAs compared to those transfected with the control siRNA (Fig. 6D–E), In contrary, the stimulating effect of APOE was not observed in OVCA433, which expressed low levels of endogenous LRP5 (Supplementary Fig. 11A and Fig. 6F). These findings suggest that LRP5 mediates the growth stimulating effect of APOE in HGSC cells, and APOE-LRP5 crosstalk could play a crucial role in modulating the survival of HGSC cells.

DISCUSSION

In this study, spatial transcriptomics technology was used to characterize CAF heterogeneity in advanced-stage HGSC. We found the absence of specific CAF subtypes in the tumor tissue of patients with advanced HGSC to be associated with survival durations of more than 10 years. Furthermore, specific ligand-receptor interactions between various tumor and CAF clusters in STS samples compared with those in LTS samples were identified.

Although most ovarian cancer patients have a median survival duration of less than 5 years, approximately 15% of patients survive more than 7 years (7). These patients are generally defined as long-term survivors (LTSs) (42). In previous studies, multiple transcriptome analyses of LTS samples were performed to identify conserved genomic signatures associated with long-term survival; however, each study identified different gene sets, most likely because of the use of heterogenous patient cohorts and the use of bulk tissue samples with various amount of stromal tissue (23). The gene sets identified may not

represent the biology of the tumor that contribute to long-term survival. In the present study, to eliminate the confounding factors associated with patient survival, we included only optimally debulked, advanced-stage, treatment-naïve HGSC samples. The use of a spatially resolved transcriptomic platform can also eliminate the issue of tissue heterogeneity among different specimens.

Our spatial transcriptomics analysis demonstrated the presence of different tumor clusters represented by different transcriptome signatures within a tumor tissue, suggesting high levels of heterogeneity not only among different HGSC samples but also within single HGSC samples. For example, several tumor clusters identified in STS but not in LTS samples expressed high levels of CDK1 and LGR5, respectively, which suggests that a cluster of tumor cells with CDK1 or LGR5 expression in the tumor tissue of an STS sample expressing one of these genes may play a role in conferring the malignant phenotype of HGSC in STSs. Indeed, several studies have shown that CDK1 dysregulation leads to robust tumor growth, chromosomal instability, and a high rate of tumor cell proliferation (43). Furthermore, other studies have demonstrated that LGR5 expression levels are positively correlated with cancer stem cell traits, shorter survival times, and chemoresistance (44,45).

Increasing evidence suggests that the stromal component of the TME plays an important role in ovarian cancer development. In HGSC patients, the high number of stromal cell types in the ovarian TME is significantly associated with poor survival (46,47). Recently, Stur et al. used spatial transcriptomics to identify spatially resolved biomarkers that can be used to differentiate between HGSC patients whose disease has a poor or excellent response to chemotherapy (48). They demonstrated the importance of the stromal component and the presence of different clusters as drivers of poor response (48). However, the clusters they identified were not annotated, and the expression of marker genes in the clusters were not validated at the protein level. Nevertheless, the authors demonstrated the feasibility of using spatial transcriptomics to identify predictive markers of treatment response. In the present study, our spatial transcriptomics analysis of treatment-naïve STS and LTS samples demonstrated high levels of both intra- and inter-stromal heterogeneity among HGSCs. Annotated stroma clusters, which were identified predominantly in STS samples, had high levels of both periostin and CD36 expression as well as high levels of COL1A1 expression. We were able to validate these findings in a larger cohort of patients using mIF analysis, which revealed a significantly higher level of periostin protein expression in a specific stroma compartment of STS samples than in that of LTS samples. Markedly higher levels of CD36 protein expression were also observed in STS. Periostin, a component of the extracellular matrix, is expressed by fibroblasts in normal tissue and by those in the stroma of various primary tumors. Periostin is also required for cancer stem cell maintenance, and blocking its function prevents metastasis (49). Periostin is also associated with poor prognosis and platinum resistance in epithelial ovarian cancer (50). CD36 fuels tumor metastasis and therapy resistance by enhancing lipid uptake and fatty acid oxidation. It also attenuates angiogenesis by binding to thrombospondin 1 and thereby inducing apoptosis or blocking the VEGFR-2 pathway in tumor and endothelial cells. Moreover, CD36-driven lipid metabolic reprogramming and functions in tumor-associated immune cells lead to tumor immune tolerance and cancer development (51). Therefore, the overexpression of

periostin and CD36 in the stromal compartment could contribute to the malignant phenotype of HGSC in STS.

To further investigate whether the stromal heterogeneity we identified represents different CAF populations, we assessed the expression of canonical CAF markers in the stroma clusters we identified. Stroma clusters in STS samples expressed all traditional CAF markers, including αSMA (ACTA2), S100A4, VIM, FAP, PDGFRα, and PDGFRβ, suggesting that these clusters represent CAF clusters. However, most stroma clusters in LTS samples expressed only αSMA and VIM but no other CAF markers, suggesting that these clusters represent myofibroblasts rather than canonical CAFs. Validation studies using mIF confirmed that the density of CAFs expressing αSMA, VIM, and PDGFRB in LTS samples was significantly lower than that in STS samples, indicating that the absence of CAF clusters that express all the canonical CAF markers can be used to predict long-term survival (Fig. 7). Although several reports identify CAF subtypes associated with poor immune infiltration and patient survival, in HGSC there is a lack of consensus markers to define CAF subtypes (16,46,47,52). Our results are in line with findings from previous studies, which demonstrated the association of some of the CAF markers we used with poor immune infiltration and patient survival (16,46,47,52). To our knowledge, our study shows for the first time an in-depth characterization of the CAF subtypes with spatial context in HGSC TME at both mRNA and protein levels.

The immune system is also an important component of the TME. Recent studies demonstrated that $CD8^+$ tumor-infiltrating lymphocytes (TILs) are associated with improved overall survival in several solid tumors, including ovarian cancer (10,11,53). Other prognostically favorable lymphocyte subsets include $CD4^+$ T cells, memory B cells, and plasma cells. These lymphocyte subsets appear to work cooperatively, as the highest patient overall survival rates are associated with tumors containing all four cell types (12). Our spatial transcriptomics analysis revealed higher densities of $CD4^+$ central memory, $CD8^+$ effector memory, monocytes, NK, B, myeloid DCs and plasmacytoid dendritic cells infiltrated in the tumor compartment of LTS than those in STS. These findings together with the identification of specific CAF subtypes in STS suggest that $SMA^+VIM^+PDGFRB^+$ CAFs in STS could create a barrier that hampers immune cells to infiltrate into the tumor mass leading to immune evasion (Fig. 7).

We characterized region-specific ligand-receptor interactions by analyzing crosstalk signaling in neighboring spots at the stroma-tumor interface. Crosstalk analysis methods have been designed for use with both cell-specific RNA-seq data (e.g., CCCexplorer (35)) and single-cell RNA-seq data (54,55). For spatial transcriptomics data, however, there is a lack of systemic approaches for analyzing the cell-cell crosstalk. In this study, we developed and applied a method for identifying region-specific ligand-receptor interactions at the stroma-tumor interface. The method can also be used to analyze crosstalk between other cell types (e.g., between tumor cells and immune cells, between cells in the immune stroma, between different tumor cells). Using this method and subsequent validation studies by mIF, we found a significant positive correlation between $LRP5^+$ cells and APOE intensity in only STS samples in which this ligand-receptor pair is exclusively expressed at the stroma-tumor interface. Further functional studies demonstrated that LRP5 mediates the growth

stimulating effect of APOE in HGSC cells. These findings suggest that a strong crosstalk signaling network between tumor-derived LRP5 and CAF-derived APOE may confer a more aggressive phenotype of the HGSC, which contribute to poorer patient survival rates (Fig. 7). Indeed, increased levels of LRP5 have been linked to metastasis in various tumor types (56–58). Moreover, APOE has been reported to be required for cell proliferation and survival in ovarian cancer and has been associated with aggressive biology and poor prognosis in colorectal cancers (59,60).

One of the limitations in the present study was that only 4 samples (2 STS samples and 2 LTS samples) were used in the initial spatial transcriptomics analysis. However, mIF analysis in a larger cohort of independent samples validated our findings, suggesting that our analytical methods were robust and stringent. The study had a small sample size owing to the rarity of treatment-naïve LTSs with advanced HGSC available (7). The use of spatial transcriptomics platforms with a more homogenous patient cohort will certainly increase the likelihood of identifying reliable prognostic or predictive biomarkers of advanced HGSC.

In conclusion, our spatial transcriptomics analysis revealed high levels of inter- and intratumor CAF heterogeneity, and novel spatially resolved CAF-tumor crosstalk signaling networks in the ovarian TME that are associated with long-term survival in patients with advanced HGSC (Fig. 7). Further elucidating the association between these spatially resolved biomarkers and long-term survival could contribute to our understanding of ovarian cancer pathogenesis and thereby improve the survival of patients with advanced HGSC.

Supplementary Material

Refer to Web version on PubMed Central for supplementary material.

ACKNOWLEDGMENTS

We are grateful for the generous donation of tissue samples by patients undergoing surgery. We thank Siu Fee Rita and Mansi Diwanji for excellent technical support with mIF slide staining. We are also grateful to Joseph Munch from the Scientific Publications, Research Medical Library at MD Anderson Cancer Center for editing the manuscript and Jordan Pietz from the Creative communications at MD Anderson Cancer Center for preparing the summary figure.

FINANCIAL SUPPORT

This study was supported in part by grants from the U.S. Department of Defense Ovarian Cancer Research Program (W81XWH-17-1-0126 and W81XWH-16-1-0038), the National Institutes of Health (U01 CA253553), the National Institutes of Health through M. D. Anderson's Cancer Center Support Grant CA016672, the NCI's Research Specialist 1 R50 CA243707-01A1, and the Tsing Tsung and Wei Fong Chao Foundation, Stephanie C. Stelter Foundation, John S. Dunn Research Foundation, and Carole Walter Looke Fund. YZ was supported by a Computational Cancer Biology Training Program fellowship CPRIT Grant No. RP170593. S.F.B. was supported by the Ovarian Cancer Research Alliance (811621). This study used MD Anderson's Flow Cytometry and Cellular Imaging Facility and its Advanced Technology Genomics Core, which are supported in part by the National Institutes of Health through MD Anderson's Cancer Center Support Grant (P30 CA016672).

REFERENCES

1. Kim J, Park EY, Kim O, Schilder JM, Coffey DM, Cho C-H, et al. Cell Origins of High-Grade Serous Ovarian Cancer. Cancers (Basel) [Internet]. 2018 [cited 2019 Feb 18];10. Available from: https://www.ncbi.nlm.nih.gov/pmc/articles/PMC6267333/

2. Siegel RL, Miller KD, Fuchs HE, Jemal A. Cancer statistics, 2022. CA: A Cancer Journal for Clinicians. 2022;72:7–33. [PubMed: 35020204]

3. Peres LC, Cushing-Haugen KL, Köbel M, Harris HR, Berchuck A, Rossing MA, et al. Invasive Epithelial Ovarian Cancer Survival by Histotype and Disease Stage. J Natl Cancer Inst. Oxford Academic; 2019;111:60–8. [PubMed: 29718305]

4. Miller DS, Blessing JA, Krasner CN, Mannel RS, Hanjani P, Pearl ML, et al. Phase II Evaluation of Pemetrexed in the Treatment of Recurrent or Persistent Platinum-Resistant Ovarian or Primary Peritoneal Carcinoma: A Study of the Gynecologic Oncology Group. J Clin Oncol. 2009;27:2686–91. [PubMed: 19332726]

5. Yeung T-L, Leung CS, Yip K-P, Au Yeung CL, Wong STC, Mok SC. Cellular and molecular processes in ovarian cancer metastasis. A Review in the Theme: Cell and Molecular Processes in Cancer Metastasis. Am J Physiol Cell Physiol. 2015;309:C444–56. [PubMed: 26224579]

6. Cress RD, Chen YS, Morris CR, Petersen M, Leiserowitz GS. Characteristics of Long-Term Survivors of Epithelial Ovarian Cancer. Obstet Gynecol. 2015;126:491–7. [PubMed: 26244529]

7. Hoppenot C, Eckert MA, Tienda SM, Lengyel E. Who are the long-term survivors of high grade serous ovarian cancer? Gynecologic Oncology. 2018;148:204–12. [PubMed: 29128106]

8. Zhang B, Chen F, Xu Q, Han L, Xu J, Gao L, et al. Revisiting ovarian cancer microenvironment: a friend or a foe? Protein Cell. 2018;9:674–92. [PubMed: 28929459]

9. Zhang L, Conejo-Garcia JR, Katsaros D, Gimotty PA, Massobrio M, Regnani G, et al. Intratumoral T cells, recurrence, and survival in epithelial ovarian cancer. N Engl J Med. 2003;348:203–13. [PubMed: 12529460]

10. Sato E, Olson SH, Ahn J, Bundy B, Nishikawa H, Qian F, et al. Intraepithelial CD8+ tumor-infiltrating lymphocytes and a high CD8+/regulatory T cell ratio are associated with favorable prognosis in ovarian cancer. Proc Natl Acad Sci USA. 2005;102:18538–43. [PubMed: 16344461]

11. Immunopathogenesis of ovarian cancer - Minerva Medica 2009 October;100(5):357-70 - Minerva Medica - Journals [Internet]. [cited 2020 Apr 3]. Available from: https://www.minervamedica.it/en/journals/minerva-medica/article.php?cod=R10Y2009N05A0357

12. Kroeger DR, Milne K, Nelson BH. Tumor-Infiltrating Plasma Cells Are Associated with Tertiary Lymphoid Structures, Cytolytic T-Cell Responses, and Superior Prognosis in Ovarian Cancer. Clin Cancer Res. American Association for Cancer Research; 2016;22:3005–15. [PubMed: 26763251]

13. Zhu Y, Ferri-Borgogno S, Sheng J, Yeung T-L, Burks JK, Cappello P, et al. SIO: A Spatioimageomics Pipeline to Identify Prognostic Biomarkers Associated with the Ovarian Tumor Microenvironment. Cancers. Multidisciplinary Digital Publishing Institute; 2021;13:1777. [PubMed: 33917869]

14. Wang W, Kryczek I, Dostál L, Lin H, Tan L, Zhao L, et al. Effector T Cells Abrogate Stroma-Mediated Chemoresistance in Ovarian Cancer. Cell. 2016;165:1092–105. [PubMed: 27133165]

15. Laumont CM, Wouters MCA, Smazynski J, Gierc NS, Chavez EA, Chong LC, et al. Single-cell Profiles and Prognostic Impact of Tumor-Infiltrating Lymphocytes Coexpressing CD39, CD103, and PD-1 in Ovarian Cancer. Clinical Cancer Research. 2021;27:4089–100. [PubMed: 33963000]

16. Han C, Liu T, Yin R. Biomarkers for cancer-associated fibroblasts. Biomarker Research. 2020;8:64. [PubMed: 33292666]

17. Öhlund D, Handly-Santana A, Biffi G, Elyada E, Almeida AS, Ponz-Sarvise M, et al. Distinct populations of inflammatory fibroblasts and myofibroblasts in pancreatic cancer. J Exp Med. 2017;214:579–96. [PubMed: 28232471]

18. Özdemir BC, Pentcheva-Hoang T, Carstens JL, Zheng X, Wu C-C, Simpson T, et al. Depletion of Carcinoma-Associated Fibroblasts and Fibrosis Induces Immunosuppression and Accelerates Pancreas Cancer with Diminished Survival. Cancer Cell. 2014;25:719–34. [PubMed: 24856586]

19. Rhim AD, Oberstein PE, Thomas DH, Mirek ET, Palermo CF, Sastra SA, et al. Stromal elements act to restrain, rather than support, pancreatic ductal adenocarcinoma. Cancer Cell. 2014;25:735–47. [PubMed: 24856585]

20. Etemadmoghadam D, deFazio A, Beroukhim R, Mermel C, George J, Getz G, et al. Integrated Genome-wide DNA Copy Number and Expression Analysis Identifies Distinct Mechanisms of Primary Chemo-resistance in Ovarian Carcinomas. Clin Cancer Res. 2009;15:1417–27. [PubMed: 19193619]

21. Zhang H, Liu T, Zhang Z, Payne SH, Zhang B, McDermott JE, et al. Integrated proteogenomic characterization of human high grade serous ovarian cancer. Cell. 2016;166:755–65. [PubMed: 27372738]
22. Patch A-M, Christie EL, Etemadmoghadam D, Garsed DW, George J, Fereday S, et al. Whole–genome characterization of chemoresistant ovarian cancer. Nature. Nature Publishing Group; 2015;521:489–94. [PubMed: 26017449]
23. Schwede M, Waldron L, Mok SC, Wei W, Basunia A, Merritt MA, et al. The Impact of Stroma Admixture on Molecular Subtypes and Prognostic Gene Signatures in Serous Ovarian Cancer. Cancer Epidemiology, Biomarkers & Prevention. 2020;29:509–19.
24. Shih AJ, Menzin A, Whyte J, Lovecchio J, Liew A, Khalili H, et al. Identification of grade and origin specific cell populations in serous epithelial ovarian cancer by single cell RNA-seq. PLOS ONE. Public Library of Science; 2018;13:e0206785. [PubMed: 30383866]
25. Izar B, Tirosh I, Stover EH, Wakiro I, Cuoco MS, Alter I, et al. A single-cell landscape of high-grade serous ovarian cancer. Nature Medicine. Nature Publishing Group; 2020;1–9.
26. Winterhoff BJ, Maile M, Mitra AK, Sebe A, Bazzaro M, Geller MA, et al. Single cell sequencing reveals heterogeneity within ovarian cancer epithelium and cancer associated stromal cells. Gynecologic Oncology. 2017;144:598–606. [PubMed: 28111004]
27. Vázquez-García I, Uhlitz F, Ceglia N, Lim JLP, Wu M, Mohibullah N, et al. Ovarian cancer mutational processes drive site-specific immune evasion. Nature. 2022;612:778–86. [PubMed: 36517593]
28. Burks JK. A model for where we live. Cell & Gene Therapy Insights. 2021;7:1513–9.
29. Carstens JL, Correa de Sampaio P, Yang D, Barua S, Wang H, Rao A, et al. Spatial computation of intratumoral T cells correlates with survival of patients with pancreatic cancer. Nature Communications. Nature Publishing Group; 2017;8:15095.
30. Gartrell RD, Marks DK, Hart TD, Li G, Davari DR, Wu A, et al. Quantitative Analysis of Immune Infiltrates in Primary Melanoma. Cancer Immunol Res. American Association for Cancer Research; 2018;6:481–93. [PubMed: 29467127]
31. Gartrell-Corrado RD, Chen AX, Rizk EM, Marks DK, Bogardus MH, Hart TD, et al. Linking Transcriptomic and Imaging Data Defines Features of a Favorable Tumor Immune Microenvironment and Identifies a Combination Biomarker for Primary Melanoma. Cancer Res. American Association for Cancer Research; 2020;80:1078–87. [PubMed: 31948941]
32. Launonen I-M, Lyytikäinen N, Casado J, Anttila EA, Szabó A, Haltia U-M, et al. Single-cell tumor-immune microenvironment of BRCA1/2 mutated high-grade serous ovarian cancer. Nat Commun. 2022;13:835. [PubMed: 35149709]
33. Marx V. Method of the Year: spatially resolved transcriptomics. Nature Methods. Nature Publishing Group; 2021;18:9–14. [PubMed: 33408395]
34. Moncada R, Barkley D, Wagner F, Chiodin M, Devlin JC, Baron M, et al. Integrating microarray-based spatial transcriptomics and single-cell RNA-seq reveals tissue architecture in pancreatic ductal adenocarcinomas. Nature Biotechnology. 2020;1–10.
35. Choi H, Sheng J, Gao D, Li F, Durrans A, Ryu S, et al. Transcriptome Analysis of Individual Stromal Cell Populations Identifies Stroma-Tumor Crosstalk in Mouse Lung Cancer Model. Cell Reports. 2015;10:1187–201. [PubMed: 25704820]
36. Yeung T-L, Sheng J, Leung CS, Li F, Kim J, Ho SY, et al. Systematic Identification of Druggable Epithelial–Stromal Crosstalk Signaling Networks in Ovarian Cancer. J Natl Cancer Inst. 2019;111:272–82. [PubMed: 29860390]
37. Shih AJ, Menzin A, Whyte J, Lovecchio J, Liew A, Khalili H, et al. Identification of grade and origin specific cell populations in serous epithelial ovarian cancer by single cell RNA-seq. PLoS One [Internet]. 2018 [cited 2020 Nov 16];13. Available from: https://www.ncbi.nlm.nih.gov/pmc/articles/PMC6211742/
38. Nath A, Cosgrove PA, Mirsafian H, Christie EL, Pflieger L, Copeland B, et al. Evolution of core archetypal phenotypes in progressive high grade serous ovarian cancer. Nat Commun. Nature Publishing Group; 2021;12:3039. [PubMed: 34031395]
39. Waltman L, van Eck NJ. A smart local moving algorithm for large-scale modularity-based community detection. Eur Phys J B. 2013;86:471.

40. Azizi E, Carr AJ, Plitas G, Cornish AE, Konopacki C, Prabhakaran S, et al. Single-Cell Map of Diverse Immune Phenotypes in the Breast Tumor Microenvironment. Cell. 2018;174:1293–1308.e36. [PubMed: 29961579]
41. Hellström I, Raycraft J, Hayden-Ledbetter M, Ledbetter JA, Schummer M, McIntosh M, et al. The HE4 (WFDC2) protein is a biomarker for ovarian carcinoma. Cancer Res. 2003;63:3695–700. [PubMed: 12839961]
42. Baldwin LA, Huang B, Miller RW, Tucker T, Goodrich ST, Podzielinski I, et al. Ten-Year Relative Survival for Epithelial Ovarian Cancer. Obstetrics & Gynecology. 2012;120:612–8. [PubMed: 22914471]
43. Izadi S, Nikkhoo A, Hojjat-Farsangi M, Namdar A, Azizi G, Mohammadi H, et al. CDK1 in Breast Cancer: Implications for Theranostic Potential. Anti-Cancer Agents in Medicinal Chemistry. 20:758–67. [PubMed: 32013835]
44. Xu L, Lin W, Wen L, Li G. Lgr5 in cancer biology: functional identification of Lgr5 in cancer progression and potential opportunities for novel therapy. Stem Cell Research & Therapy. 2019;10:219.
45. Cao H-Z, Liu X-F, Yang W-T, Chen Q, Zheng P-S. LGR5 promotes cancer stem cell traits and chemoresistance in cervical cancer. Cell Death Dis. Nature Publishing Group; 2017;8:e3039–e3039. [PubMed: 28880275]
46. Heindl A, Lan C, Rodrigues DN, Koelble K, Yuan Y. Similarity and diversity of the tumor microenvironment in multiple metastases: critical implications for overall and progression-free survival of high-grade serous ovarian cancer. Oncotarget. 2016;7:71123–35. [PubMed: 27661102]
47. Lan C, Heindl A, Huang X, Xi S, Banerjee S, Liu J, et al. Quantitative histology analysis of the ovarian tumour microenvironment. Sci Rep. Nature Publishing Group; 2015;5:16317. [PubMed: 26573438]
48. Stur E, Corvigno S, Xu M, Chen K, Tan Y, Lee S, et al. Spatially resolved transcriptomics of high-grade serous ovarian carcinoma. iScience [Internet]. Elsevier; 2022 [cited 2022 Mar 21];25. Available from: https://www.cell.com/iscience/abstract/S2589-0042(22)00193-6
49. Malanchi I, Santamaria-Martínez A, Susanto E, Peng H, Lehr H-A, Delaloye J-F, et al. Interactions between cancer stem cells and their niche govern metastatic colonization. Nature. Nature Publishing Group; 2012;481:85–9.
50. Sung P-L, Jan Y-H, Lin S-C, Huang C-C, Lin H, Wen K-C, et al. Periostin in tumor microenvironment is associated with poor prognosis and platinum resistance in epithelial ovarian carcinoma. Oncotarget. Impact Journals; 2015;7:4036–47.
51. Wang J, Li Y. CD36 tango in cancer: signaling pathways and functions. Theranostics. 2019;9:4893–908. [PubMed: 31410189]
52. Zou R, Jiang Q, Jin T, Chen M, Yao L, Ding H. Pan-cancer analyses and molecular subtypes based on the cancer-associated fibroblast landscape and tumor microenvironment infiltration characterization reveal clinical outcome and immunotherapy response in epithelial ovarian cancer. Front Immunol. 2022;13:956224. [PubMed: 36032075]
53. Zhang L, Conejo-Garcia JR, Katsaros D, Gimotty PA, Massobrio M, Regnani G, et al. Intratumoral T Cells, Recurrence, and Survival in Epithelial Ovarian Cancer. New England Journal of Medicine. Massachusetts Medical Society; 2003;348:203–13. [PubMed: 12529460]
54. Efremova M, Vento-Tormo M, Teichmann SA, Vento-Tormo R. CellPhoneDB: inferring cell–cell communication from combined expression of multi-subunit ligand–receptor complexes. Nat Protoc. Nature Publishing Group; 2020;15:1484–506. [PubMed: 32103204]
55. Browaeys R, Saelens W, Saeys Y. NicheNet: modeling intercellular communication by linking ligands to target genes. Nat Methods. Nature Publishing Group; 2020;17:159–62. [PubMed: 31819264]
56. Rabbani SA, Arakelian A, Farookhi R. LRP5 knockdown: effect on prostate cancer invasion growth and skeletal metastasis in vitro and in vivo. Cancer Med. 2013;2:625–35. [PubMed: 24403228]
57. Hoang BH, Kubo T, Healey JH, Sowers R, Mazza B, Yang R, et al. Expression of LDL receptor-related protein 5 (LRP5) as a novel marker for disease progression in high-grade osteosarcoma. Int J Cancer. 2004;109:106–11. [PubMed: 14735475]

58. Chin EN, Martin JA, Kim S, Fakhraldeen SA, Alexander CM. Lrp5 Has a Wnt-Independent Role in Glucose Uptake and Growth for Mammary Epithelial Cells. Mol Cell Biol. 2016;36:871–85.

59. Chen Y-C, Pohl G, Wang T-L, Morin PJ, Risberg B, Kristensen GB, et al. Apolipoprotein E is required for cell proliferation and survival in ovarian cancer. Cancer Res. 2005;65:331–7. [PubMed: 15665311]

60. Zhao Z, Zou S, Guan X, Wang M, Jiang Z, Liu Z, et al. Apolipoprotein E Overexpression Is Associated With Tumor Progression and Poor Survival in Colorectal Cancer. Front Genet. 2018;9:650. [PubMed: 30631342]

SIGNIFICANCE

Generation of spatially resolved gene expression patterns in tumors from ovarian cancer patients surviving more than ten years allows the identification of novel predictive biomarkers and therapeutic targets for better patient management.

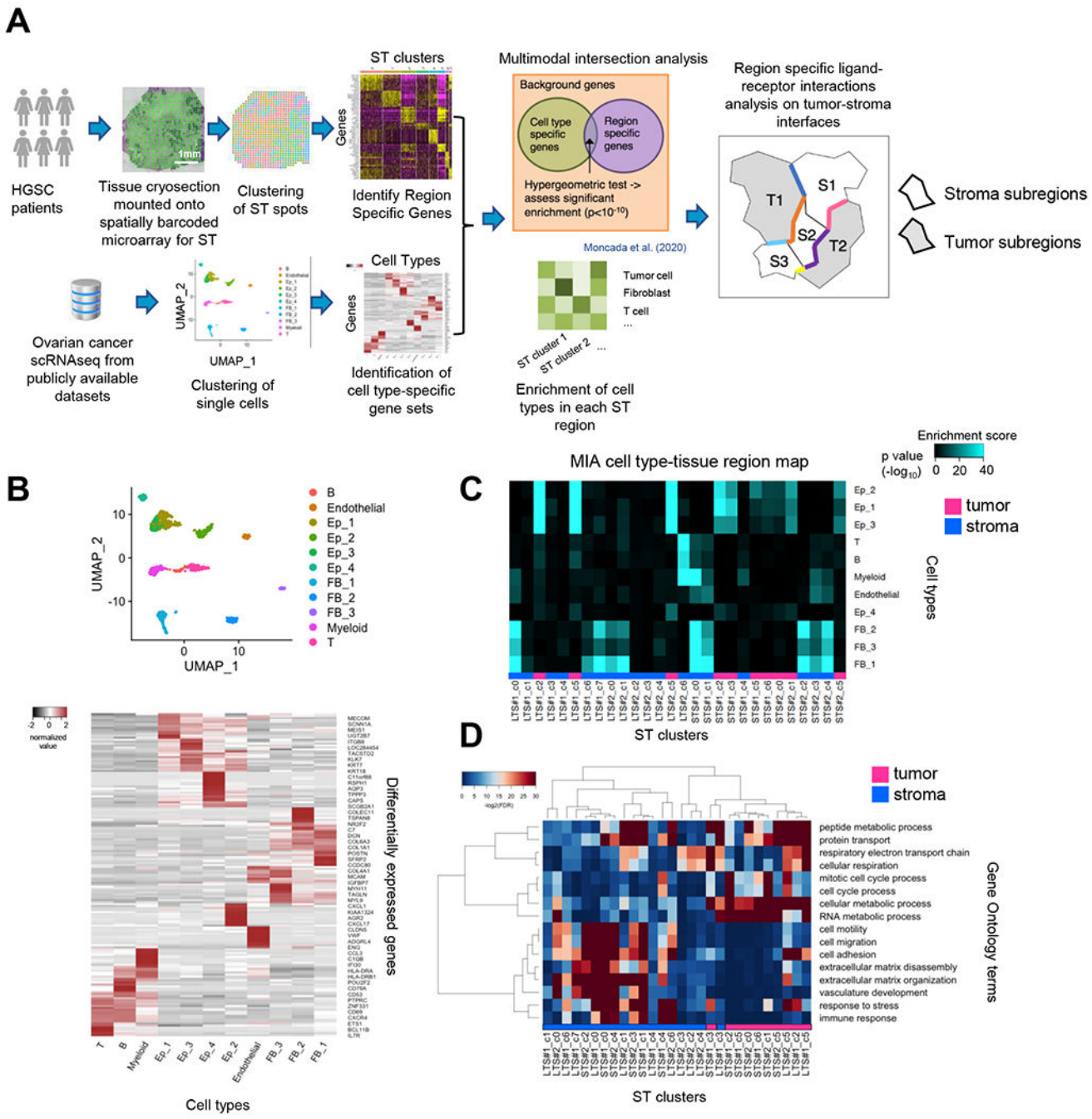

Fig. 1: Spatial transcriptomics analysis of four HGSC patient samples.

A. Schematic of the analysis workflow. The spatial transcriptomics data from our ovarian cancer patient samples were integrated with scRNA-seq data from publicly available datasets. Each spatial transcriptomics tissue cryosection was mounted onto a spatially barcoded microarray. The spots on the microarray were sequenced and clustered based on the gene expression in multiple regions. The scRNA-seq data were also clustered, which generated multiple cell types and their specific gene sets. MIA was performed to identify the overlap between region-specific genes and cell type–specific genes, and a hypergeometric

test was performed to determine whether the overlap was significant. The $-\log_{10}$(p-value) of the test was used to estimate the enrichment of a cell type in that region. The region-specific ligand-receptor interactions between adjacent stroma and tumor clusters were analyzed. **B.** Top, clustering of scRNA-seq data (n=1,156 cells; data from GSE118828). scRNA-seq data were analyzed and used to define differentially expressed genes for the major cell types. For each cell type, genes whose expression was statistically higher in the cells annotated to that cell type in comparison with their expression in the remaining cells were identified ($p < 0.00001$, Wilcoxon rank sum test, average log_fold-change > 0.25). Bottom, heatmap of the top 15 differentially expressed genes in each cluster. **C.** The MIA map of all scRNA-seq–identified cell types and spatial transcriptomics-defined regions. Each element in the matrix was computed for all pairs of cell types and tissue regions. The hypergeometric test identified tumor clusters as those enriched with any of the Ep_1, Ep_2, Ep_3, or Ep_4 cell types with a p-value of less than 1×10^{-10}. A cluster was identified as a stroma cluster if it was not a tumor cluster. The bar at the bottom indicates the region type. **D.** Overrepresentation analysis of the DAVID Gene Ontology gene sets. The bar at the bottom indicates tumor and stroma clusters, which are highlighted in magenta and blue, respectively.

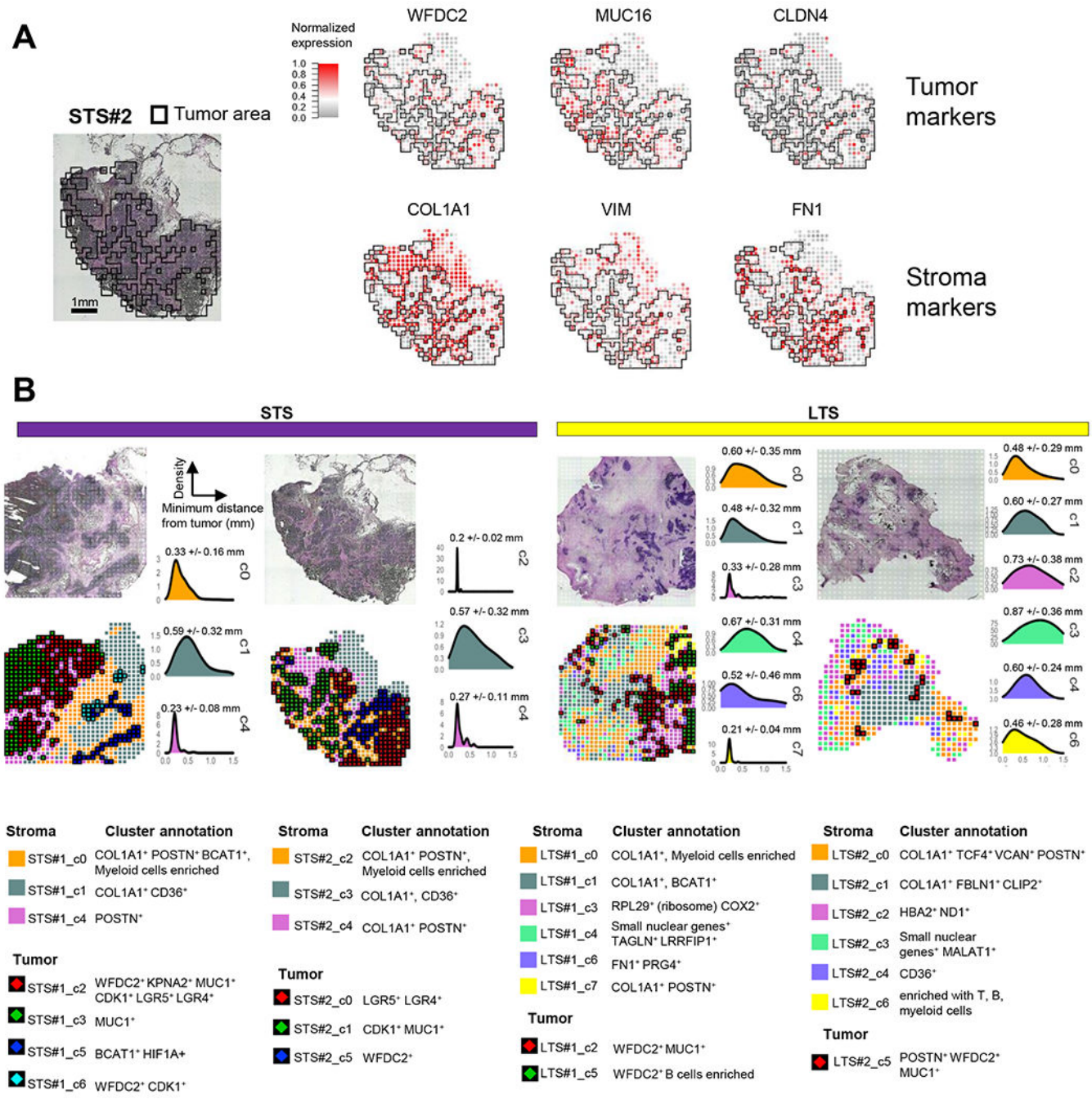

Fig. 2: Spatial transcriptomics of HGSC and mapping of clusters.

A. Spatial expression of marker genes on a representative spatial transcriptomics sample. Left, H&E staining; the tumor outline identified by MIA (black) is overlaid on the tumor regions. Right, normalized spatial expression of the tumor and stroma markers; the black outline indicates the tumor outline the same as that in the left panel. B. Top, H&E staining. Bottom, Clustering of spatial transcriptomics spots by gene expression. Clusters are annotated by marker genes of tumor and stroma, the top differentially expressed genes, and MIA enrichment analysis of Fig. 1. Samples are grouped as STS samples (left) and

LTS samples (right). For each cluster, density plots show the minimum distance from each stroma spot to the tumor spots. The mean +/− standard deviation for the density distribution is shown at the top of each plot.

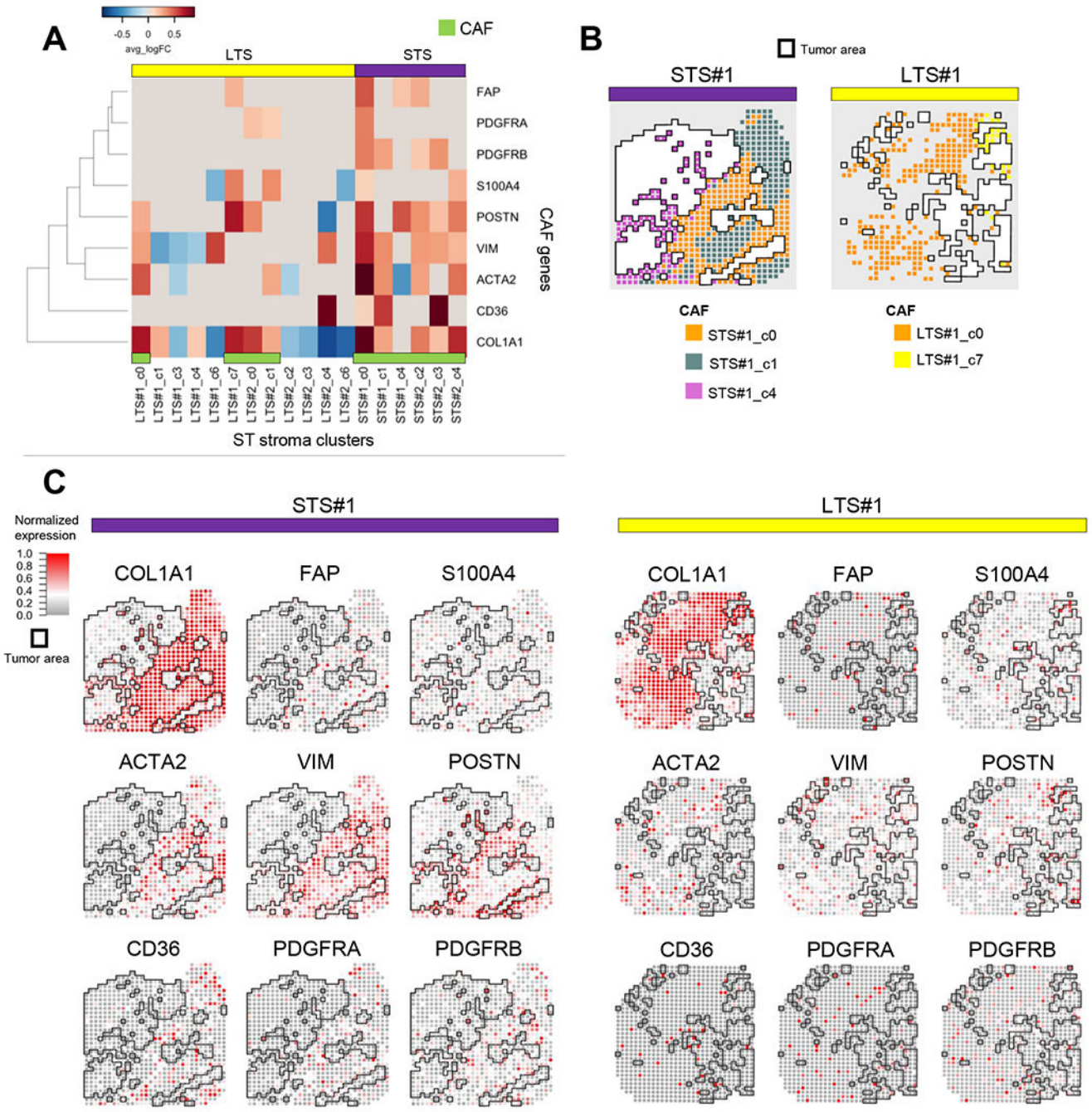

Fig. 3: Heterogeneity of CAFs.

A. Heatmap of the average log fold-change of CAF gene expression in the stroma clusters. The average log fold-change was computed as the log fold-change of the average expression of a gene between a cluster and all the other clusters of the sample. The average log fold-change was set to 0 if the p-value was larger than 0.01 (Wilcoxon rank sum test). **B.** Mapping of CAF clusters in an STS sample (left) and an LTS sample (right). **C.** Spatial expression of selected CAF genes in an STS sample (left) and an LTS sample (right).

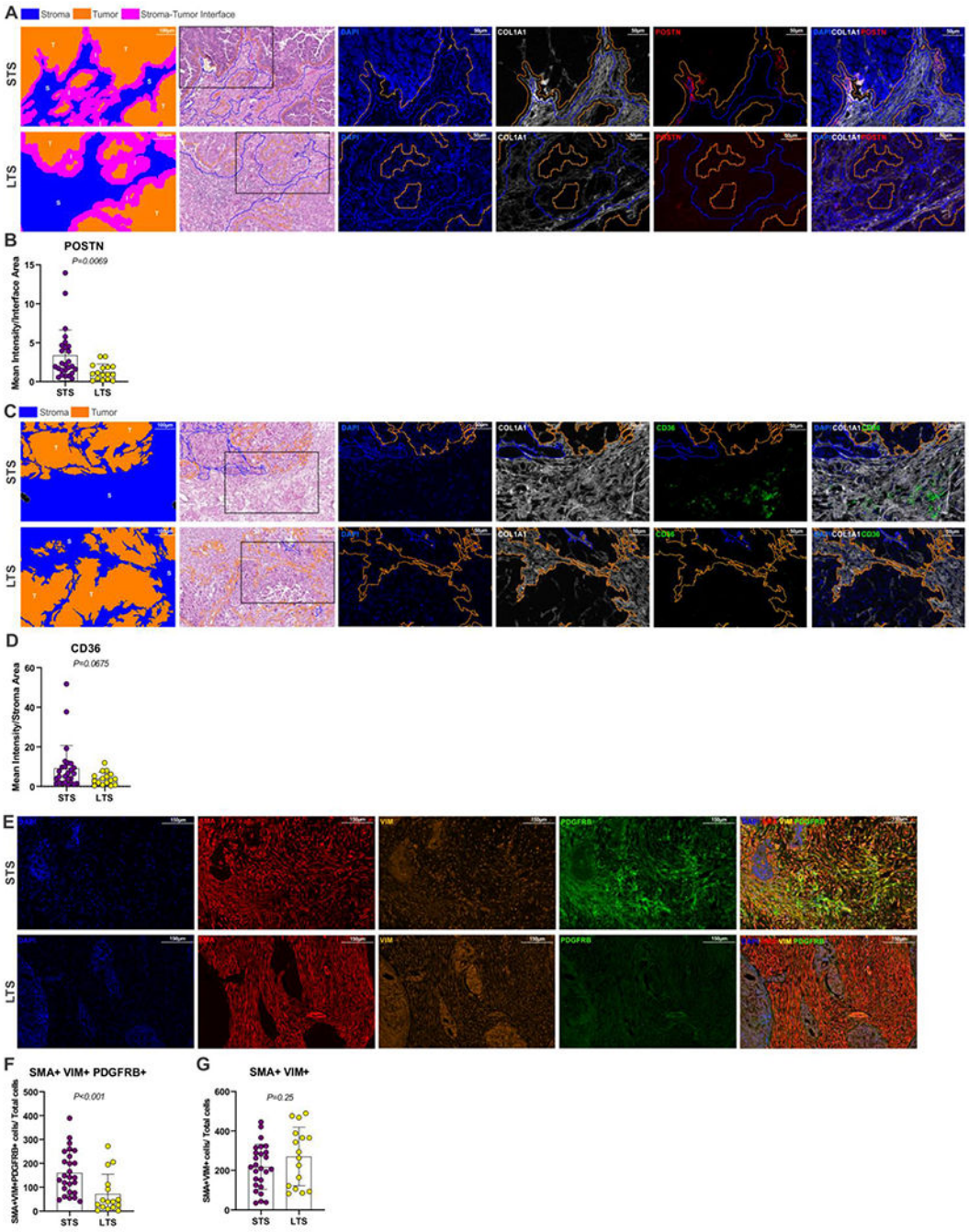

Fig. 4: Validation of CAF subclusters.

A-D. mIF staining of markers of stroma subclusters in paraffin-embedded HGSC tissue: periostin (POSTN; A-B) and CD36 (C-D). A, C. Scale bar for two left panels is 100μm, for right panels is 50μm. Black square in H&E image indicates the enlarged region in the mIF panels. Orange lines represent the tumor boundary, while blue lines represent the stroma boundary. **E-G.** mIF staining of markers of CAF subclusters. Scale bar for panel E is 150μm. Data represented as mean ± SD and two-tailed unpaired Student's t test have been used to compare STS (n = 26) and LTS (n = 16) samples and considered significant if $P < 0.05$.

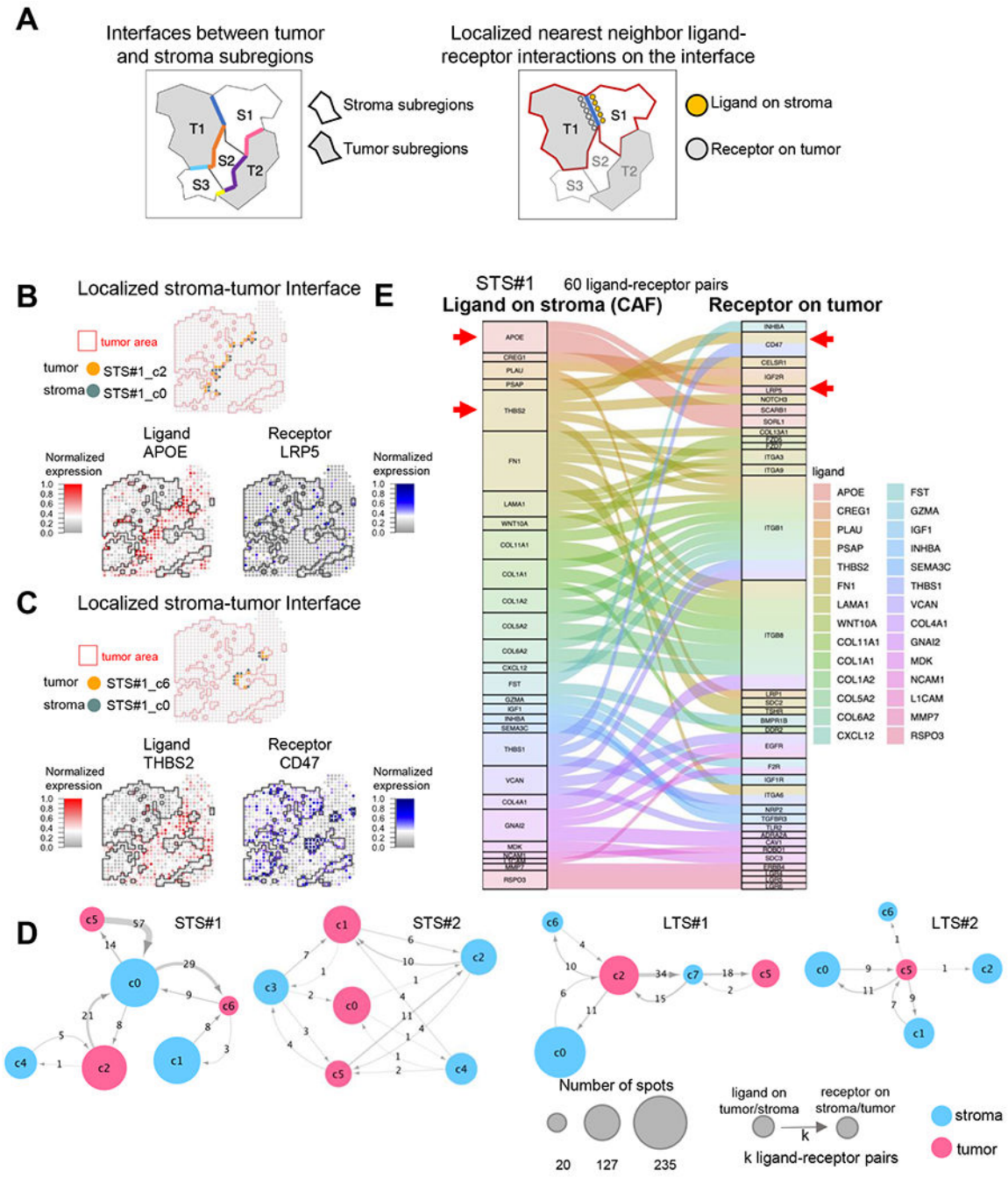

Fig. 5: Region-specific ligand-receptor interactions between stroma and tumor.

A. Illustration of the method used to identify the region-specific ligand-receptor interactions. Left, Different stroma-tumor interfaces in a sample. Right, the method identifies the ligand-receptor pairs at each interface. **B, C.** Representative nearest-neighbor interactions between tumor and stroma subregions. Top, Localization of nearest-neighbor spots of the tumor subregion (orange) and stroma subregion (gray). Red outlining indicates the tumor area of the sample. Bottom, the expressions of the ligand (left)-receptor (right) pairs are localized near the interface shown in the top panel. **D.** Nearest-neighbor interaction networks

between tumor and stroma subregions in all four samples. Pink and blue indicate tumor and stroma subregions, respectively. The node size is proportional to the number of spots in a subregion, and the width of the edges between nodes is proportional to the number of ligand-receptor pairs. **E.** Alluvial plot of all ligand-receptor pairs between tumor and stroma in a representative sample. Sixty ligand-receptor pairs were identified and pooled from all the interfaces between every stroma and tumor subregion.

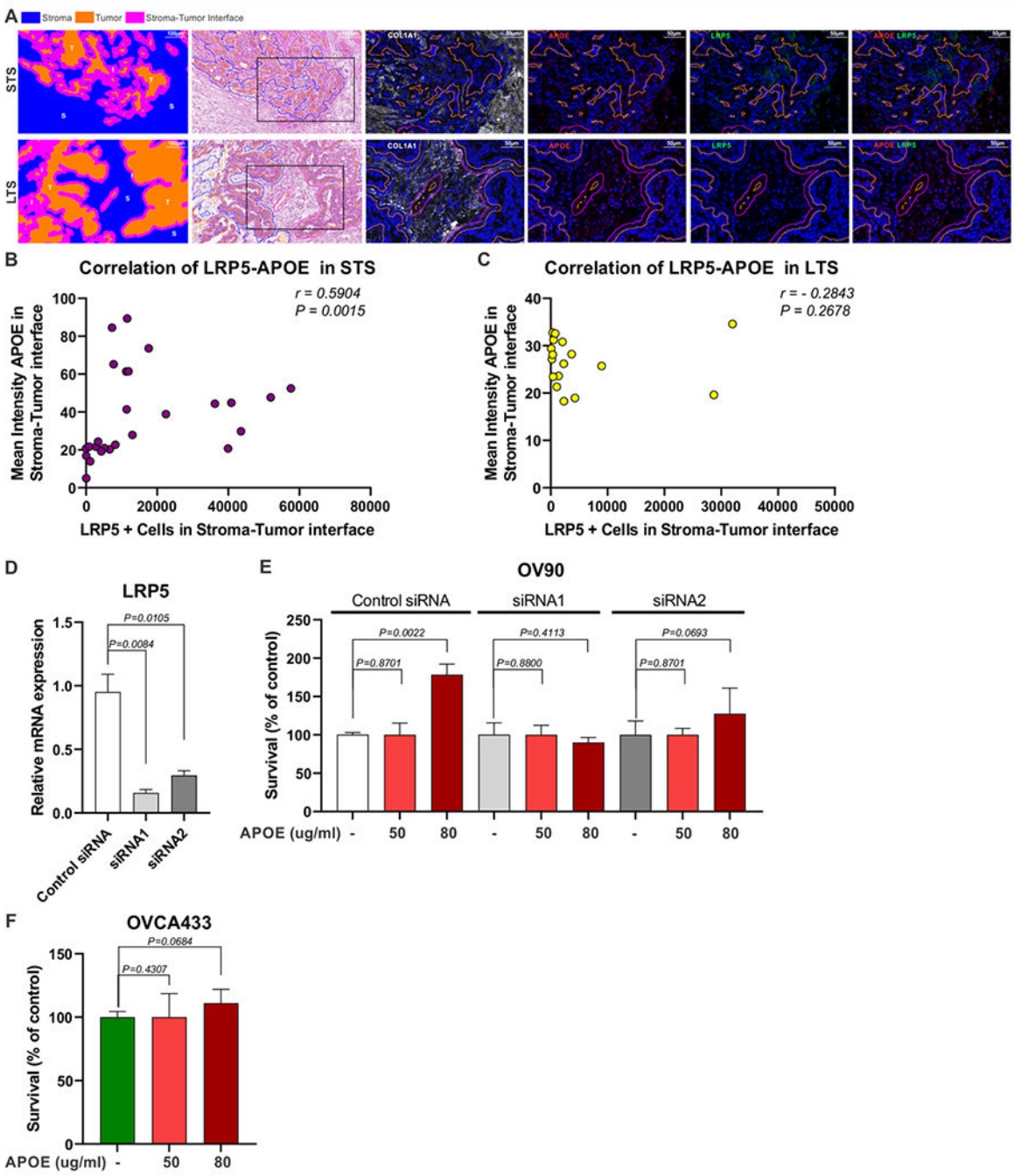

Fig. 6: Validation of ligand-receptor cross-talk at the stroma-tumor interface.

A. mIF staining of the ligand-receptor pair APOE-LRP5 in paraffin-embedded HGSC tissues. Scale bar for two left panels is 100μm, for right panels is 50μm. Black square in H&E image indicates the enlarged region in the mIF panels. Orange lines represent the tumor boundary, while blue lines represent the stroma boundary. **B, C.** Spearman's correlation analysis between $LRP5^{+}$ cells and APOE expression intensity in the stroma-tumor interface area in STS samples (B) and LTS samples (C). Two-tailed Student's t test have been used to compare STS (n = 26) and LTS (n = 16) samples and considered

significant if $P < 0.05$. **D.** Relative mRNA expression of LRP5 in a HGSC cell line (OV90) 24h after siRNA transfection. **E, F.** MTT assay after 48h treatment with APOE protein or control buffer with OV90 (E) or OVCA433 cell lines (F). Three independent experiments were conducted, and data represented as mean ± SD and two-tailed unpaired Student's t test have been used for data analysis (unless otherwise indicated) and considered significant if $P < 0.05$.

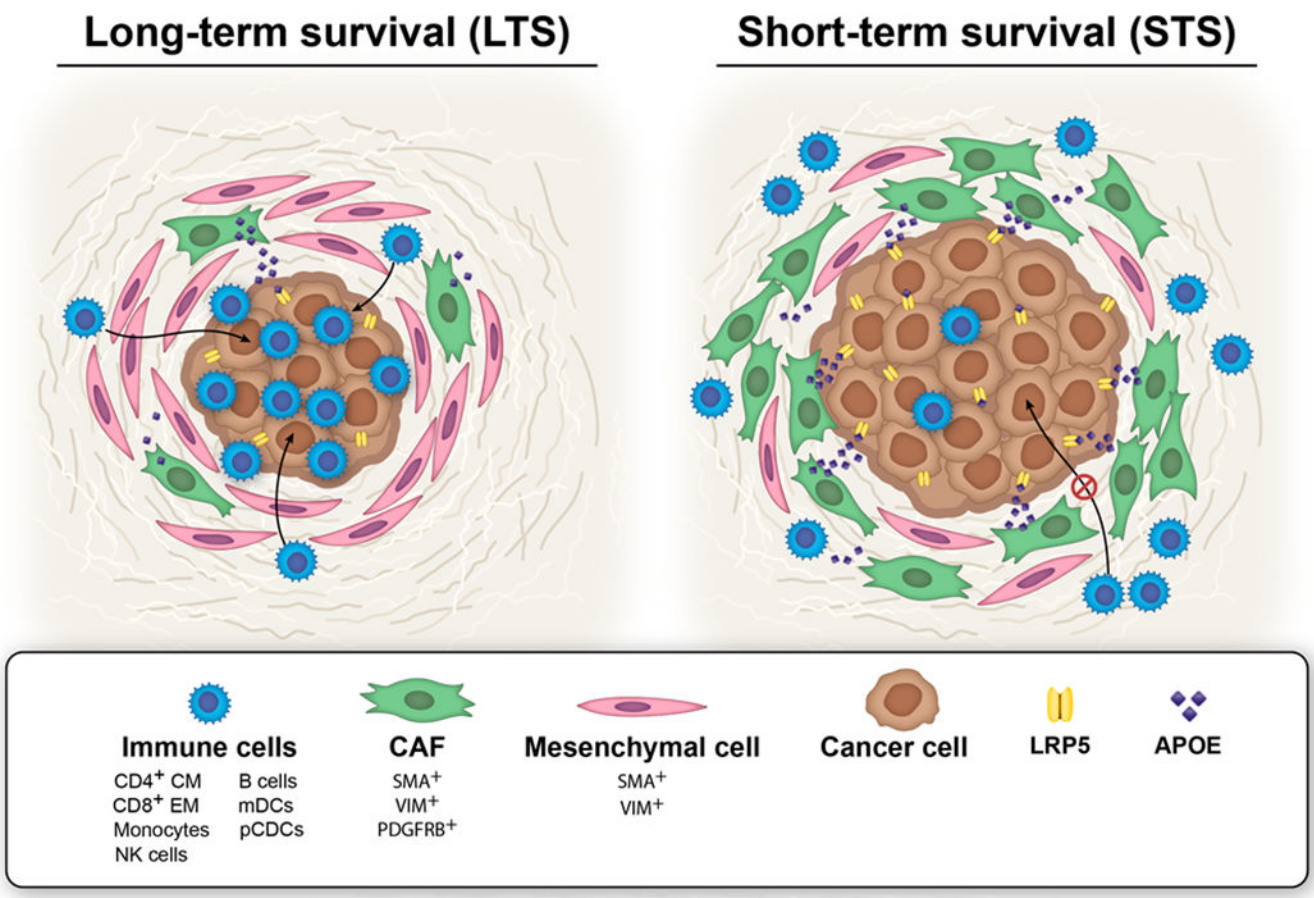

Fig. 7: Schematic summarizing the TME complexity of long- and short-term ovarian cancer survivors.

Spatial transcriptomics revealed an enrichment of $CD4^+$ central memory ($CD4^+$ CM), $CD8^+$ effector memory ($CD8^+$ EM), monocytes, natural killer (NK), B, myeloid DCs (mDCs) and plasmacytoid dendritic cells (pCDCs or pDCs) infiltrated in the tumor of LTS compared to STS. In contrast STS appear to contain a higher level of SMA+VIM+PDGFRB+ CAFs as well as more crosstalk between APOE and LRP5 at the tumor-stroma interface, which could hamper the infiltration of tumor cells and increase tumor cell proliferation and survival. Copyright used with the permission of The Board of Regents of the University of Texas System through The University of Texas MD Anderson Cancer Center.